Appendix E

Electrode Interactions in Transducers

The transducer analysis given in Chapter 4 makes use of the quasi-static approximation, which ignores the perturbation of a propagating surface wave by the electrodes of a shorted transducer. In practice each electrode reflects an incident wave to some extent, and this can be significant if the reflected waves add coherently, that is, if the electrodes are regular and the pitch is close to a multiple of the half-wavelength. The main consequences are that a shorted transducer will reflect surface waves, in contrast with the prediction of the quasi-static analysis, and that its frequency response is distorted. The electrodes also perturb the surface wave velocity, as shown by the analysis in Section D.2. These effects arise from two distinct causes: electrical loading and mechanical loading. For strongly piezoelectric materials, such as lithium niobate, electrical loading can cause severe distortions. However, mechanical loading is not usually very significant in practice, provided the metal film used for the transducer has elastic properties similar to the substrate; this condition is usually met by using an aluminium film.

To analyse electrode interactions in transducers, several types of modified equivalent network models have been used [480, 481]. In particular the crossed-field model, which in its basic form neglects electrode interactions, may be modified by introducing transmission lines to represent surface wave propagation, using different characteristic impedances in the metallised and unmetallised regions [355, 470, 482]. This model does not correctly account for the variation of electrode reflectivity with frequency and with metallisation ratio, though these limitations would be overcome if the transmission line parameters were varied in an appropriate manner. The analysis here is based on a "reflective array model", which assumes that the perturbation due to each electrode can be represented by a transmission matrix related to an effective reflection coefficient, r. The transducer properties can be deduced by cascading the transmission matrices of the electrodes. This approach has the merit of generality, since the properties of the array are related to the reflection coefficient of one electrode without invoking the physical mechanism of the reflection. The method is closely related to the analyses of Skeie [483–486], Emtage [487, 488] and Panasik and Hunsinger [489]. Another method is the generalised Green's function analysis of Milsom *et al.* [93].

Section E.1 below describes the reflective array model, and Section E.2 uses the Green's function method to deduce the reflection coefficient of one electrode due to electrical loading. The results are brought together in Section E.3, which derives the relevant transducer properties. Mechanical loading is discussed in Section E.4.

Throughout this appendix the electrodes are taken to be regular. End effects, bulk wave excitation and electrode resistivity are ignored.

E.1. Reflective Array Model

We consider an array of identical electrodes with pitch p, as shown in Figure E.1. It is assumed that any electrical connections to the electrodes are all identical, so that the electrodes will all scatter surface waves in the same manner. Here the properties of the array are deduced in terms of the scattering due to individual electrodes. The mechanism of the scattering is not considered at this stage, so the results are valid for both electrical and mechanical loading, and are also applicable to the other types of periodic structure. The analysis for an infinite structure is given in more detail by Collin [490]. An alternative approach, modelling the array as a series of repetitively mismatched transmission lines, was used by Sittig and Coquin [491] to analyse both infinite and finite structures. This gives results equivalent to those presented here.

At some frequency ω, it is assumed that the disturbance in the gaps between the electrodes includes terms of the form $\exp(\pm jk_0x)$ representing propagating waves, where k_0 is the wavenumber for surface waves on a free surface. Considering one particular electrode, the amplitudes of waves on the left are denoted by c_1 and b_1, and the amplitudes of waves on the right are denoted by c_2 and b_2, as in Figure E.1. These amplitudes are measured at points distant $p/2$ from the centre of the electrode. The terms c_1 and c_2 denote waves propagating to the right, with amplitudes proportional to $\exp(-jk_0x)$, while b_1 and b_2 denote waves propagating to the left. The amplitudes are linearly related, so that the waves leaving the electrode can be written in terms of incident waves, using a scattering matrix S_{ij}:

$$\begin{bmatrix} b_1 \\ c_2 \end{bmatrix} = \begin{bmatrix} S_{11} & S_{12} \\ S_{12} & S_{11} \end{bmatrix} \begin{bmatrix} c_1 \\ b_2 \end{bmatrix} \tag{E.1}$$

This equation uses the $= S_{11}$ and $S_{21} = S_{12}$, which follow from the

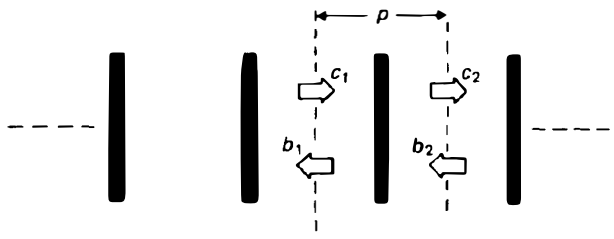

FIGURE E.1. Wave propagation in an infinite array of regular electrodes.

symmetry. If either c_1 or b_2 is zero, S_{11} gives the reflected wave amplitude, while S_{12} gives the transmitted wave amplitude. Defining r as the reflection coefficient of the electrode (referred to its centre) and t as the transmission coefficient, we have

$$S_{11} = r \exp(-jk_0p) \tag{E.2}$$

and

$$S_{12} = t \exp(-jk_0p). \tag{E.3}$$

If the electrode did not perturb the wave, we would have $r = 0$ and $t = 1$. It should be noted that r and t are defined for an electrode in a periodic array, and their values may be affected by the presence of neighbouring electrodes. This is true in the case of scattering due to electrical loading. Generally, r and t will be frequency dependent.

It is assumed here that there is no loss of power. Setting $b_2 = 0$ and equating the input power to the sum of the output powers, we have

$$|r|^2 + |t|^2 = 1. \tag{E.4}$$

In addition, if all four of the amplitudes b_1, b_2, c_1 and c_2 are non-zero, power conservation gives

$$rt^* + tr^* = 0. \tag{E.5}$$

Combining this with equation (E.4) we find

$$r^2 = t^2 - t/t^*, \tag{E.6}$$

and, using equation (E.4) again, we also have

$$r/t = \pm j|r/t|. \tag{E.7}$$

Thus the reflection and transmission coefficients are in phase quadrature. Apart from a phase ambiguity of π, the reflection coefficient can be deduced from the transmission coefficient.

For subsequent analysis it is convenient to relate the waves on the right of the electrode to those on the left by means of a transmission matrix T_{ij}, defined such that

$$\begin{bmatrix} c_2 \\ b_2 \end{bmatrix} = \begin{bmatrix} T_{11} & T_{12} \\ T_{21} & T_{22} \end{bmatrix} \begin{bmatrix} c_1 \\ b_1 \end{bmatrix} \tag{E.8}$$

The coefficients T_{ij} are obtained by re-arranging equation (E.1). Making use of equation (E.6) we find

$$[T] = \begin{bmatrix} 1/\tau^* & r/t \\ -r/t & 1/\tau \end{bmatrix}, \tag{E.9}$$

where for convenience we define $\tau = S_{12}$, the transmission coefficient for one cell of the periodic structure, so that

$$\tau = t \exp(-jk_0p). \tag{E.10}$$

Propagation in an Infinite Array. In a regular array of electrodes the above equations apply to each electrode, and the wave amplitudes c_2 and b_2 on the right of one electrode can be identified with the amplitudes c_1 and b_1 on the left of the subsequent electrode. In an infinite array, the solution corresponds to a propagating wave motion if, for each electrode, c_2 and b_2 are the same as c_1 and b_1 apart from a phase shift. Here the phase shift is taken to be $-\gamma p$, so that γ can be interpreted as the wavenumber. We thus consider solutions in which

$$\begin{aligned} c_2 &= c_1 \exp(-j\gamma p), \\ b_2 &= b_1 \exp(-j\gamma p), \end{aligned} \tag{E.11}$$

which give a propagating wave if γ is real. Using the transmission matrix, equations (E.8) and (E.9), gives a dispersion relation for γ, and with the aid of equation (E.6) we find

$$2\cos\gamma p = \frac{1}{\tau} + \frac{1}{\tau^*} \tag{E.12}$$

This can be re-arranged conveniently if we define θ_t as the phase of the electrode transmission coefficient t, so that

$$t = |t| \exp(j\theta_t), \tag{E.13}$$

We then have, from equation (E.10), $\tau = |t| \exp[j(\theta_t - k_0 p)]$, and equation (E.12) gives

$$\cos\gamma p = \frac{\cos(k_0 p - \theta_t)}{|t|}. \tag{E.14}$$

Here k_0, the free-surface wavenumber, is proportional to ω. It is usually the case that θ_t is small and $|t|$ is close to unity, so that for most values of ω there is a real solution for γ, close to $\pm k_0$. However, since $|t| < 1$ the right side of equation (E.14) is greater than 1 or less than -1 when $k_0 p$ is close to a multiple of π, and γ is then complex, giving a stop band. The solution is ambiguous in that equation (E.14) remains valid if a multiple of $2\pi/p$ is added to γ, as expected from the form of equations (E.11). In any interval of width $2\pi/p$ there are two solutions for γ, corresponding to waves propagating in opposite directions. For any particular solution the wave amplitudes c_1 and b_1 are finite, so that the solution involves waves propagating in both directions, even though the overall wave motion is in one direction.

The stop-band edges occur when the right side of equation (E.14) is equal to ± 1. Using Equation (E.4) this condition can be written

$$k_0 p - \theta_t = m\pi \pm \sin^{-1}(|r|), \quad m = 0, \pm 1, \pm 2 \ldots . \tag{E.15}$$

Here $k_0 = \omega/v_0$, where v_0 is the free-surface velocity. Usually r and θ_t vary slowly with frequency, and r is small. Thus the width in frequency of each stop band is given by

$$\Delta\omega \approx 2v_0|r|/p, \tag{E.16}$$

which is proportional to the electrode reflection coefficient. Within each stop-band, equation (E.14) is satisfied by writing γ as

$$\gamma = M\pi/p + j\alpha, \tag{E.17}$$

where α is given by

$$\cosh(\alpha p) = (-1)^M \frac{\cos(k_0 p - \theta_t)}{|t|} \tag{E.18}$$

and the integer M is chosen such that the right side of equation (E.18) is positive.

Propagation in a Finite Array. We now consider an array of N electrodes, as shown in Figure E.2. For analysis of interdigital transducers, given later, it is necessary to evaluate the amplitudes of waves propagating in the structure, and of the reflected wave, when a surface wave is incident at one end. To do this, the transmission matrix of equation (E.9) is used. It is assumed that end effects can be ignored, so that the same transmission matrix can be used for all the electrodes. Thus, for electrode n the wave amplitudes on the two sides are related by

$$\begin{bmatrix} c_n \\ b_n \end{bmatrix} = [T] \begin{bmatrix} c_{n-1} \\ b_{n-1} \end{bmatrix}, \tag{E.19}$$

where $[T]$ is given by equation (E.9) and $1 \leqslant n \leqslant N$. Applying this equation recursively to electrodes 1 to n, we have

$$\begin{bmatrix} c_n \\ b_n \end{bmatrix} = [T]^n \begin{bmatrix} c_0 \\ b_0 \end{bmatrix}, \tag{E.20}$$

which relates the waves to the right of electrode n to the waves at the left end of the array. Now, for any 2×2 matrix $[T]$, the elements of the matrix $[T]^n$ can be written in terms of the elements of $[T]$, using formulae given in References [491–493]. Denoting the elements of $[T]^n$ by T_{ij}^n, we have in the present case

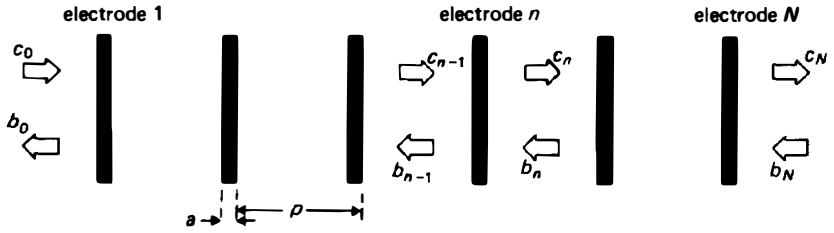

FIGURE E.2. Wave propagation in a finite array of regular electrodes.

$$T_{11}^n = \frac{\sin(n\gamma p) - \tau^* \sin[(n-1)\gamma p]}{\tau^* \sin(\gamma p)}$$

$$T_{12}^n = -T_{21}^n = \frac{r}{t}\frac{\sin(n\gamma p)}{\sin(\gamma p)},$$

$$T_{22}^n = \frac{\sin(n\gamma p) - \tau \sin[(n-1)\gamma p]}{\tau \sin(\gamma p)}, \tag{E.21}$$

where γ is the propagation constant for waves in an infinite array, given by equation (E.14). These equations are readily verified by calculating the product $[T]^n[T]$, which is found to be equal to $[T]^{n+1}$.

If there is only one incident wave, at the left of the structure, we have $b_N = 0$. In this case the ratio b_0/c_0 can be found from equation (E.20), setting $n = N$. Equation (E.20) may then be used to evaluate c_n/c_0 and b_n/c_0, thus giving the wave amplitudes throughout the structure. Thus, for $b_N = 0$ we find

$$\frac{c_n}{} = \frac{\sin(N-n)\gamma p - \tau \sin(N-n-1)\gamma p}{)\gamma p} \tag{E.22}$$

and

$$\frac{}{c_0} = \frac{}{t \sin N\gamma p - \tau \sin (N-1)\gamma p}. \tag{E.23}$$

It can be shown from these equations that $|b_0|^2 + |c_N|^2 = |c_0|^2$, so that the power is conserved. If the electodes were absent we would have $r = 0$ and $t = 1$, and the above equations then give $b_n = 0$ and $c_n = c_0 \exp(-jnk_0p)$.

For $n = 0$, equation (E.23) gives the ratio b_0/c_0, which is the reflection coefficient of the array. Taking the squared modulus of this gives the power reflection coefficient, which is found to be

$$\left|\frac{b_0}{c_0}\right|^2 = \left[1 + \left|\frac{t}{r}\right|^2 \frac{\sin^2(\gamma p)}{\sin^2(N\gamma p)}\right]^{-1}. \tag{E.24}$$

The amplitude reflection coefficient $|b_0/c_0|$ is plotted as a function of $k_0 = \omega/v_0$ in Figure E.3, taking $|t/r|$ to be independent of frequency, which is usually a good approximation. For $N|r| \ll 1$ the amplitude of the reflected wave is approximately proportional to $\sin(N\gamma p)/\sin(\gamma p)$, which has the form expected when multiple reflections are negligible. For $N|r| \gg 1$ the reflection coefficient is close to unity when k_0 is in the range corresponding to the stop band for an infinite array.

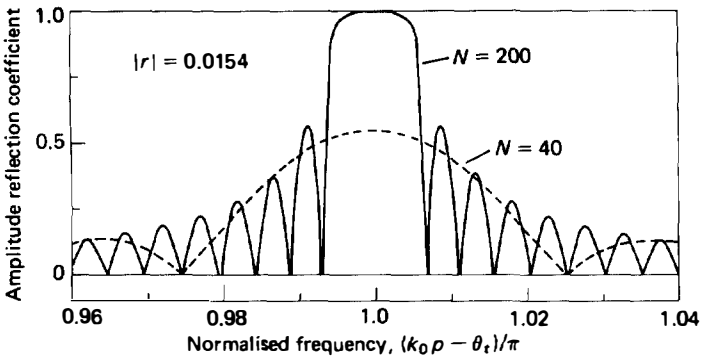

FIGURE E.3. Reflection coefficient of a finite array.

E.2. Electrode Reflection Coefficient Due to Electrical Loading

In this section we evaluate the reflection coefficient r for an electrode in an array of regular electrodes. Mechanical loading is ignored here, so that the reflection coefficient is due only to electrical loading. The analysis involves a particular electrostatic solution, which is considered first for convenience.

(a) Electrostatic Solution for an Incident Surface Wave. We consider an infinite array of regular electrodes, with pitch p and width a, on the surface of an anisotropic *non-piezoelectric* half-space. It is supposed that, in the absence of the electrode, a surface potential

$$\phi_i(x) = \phi_{i0}\, e^{-j\kappa x} \tag{E.25}$$

would be present. With the electrodes present, a charge density $\sigma_1(x)$ is generated such that the total potential, which includes the contribution $\phi_i(x)$, is uniform over each electrode. The problem here is to evaluate $\sigma_1(x)$, which will later be seen to give the first-order charge density for a shorted transducer with a surface wave incident on it. The subscript on $\sigma_1(x)$ distinguishes it from other functions required later. The derivation is very similar to the Floquet analysis of Appendix D, and is also described by Skeie [484, 486] and by Datta and Hunsinger [479]. For simplicity, it is assumed here that the constant κ in equation (E.25) is confined to the range

$$0 \leqslant \kappa \leqslant 2\pi/p. \tag{E.26}$$

Taking the electrodes to be centred at $x = np$, the charge density and the x-component of the field at the surface are written as Floquet expansions:

$$\begin{aligned} \sigma_1(x) &= \sum_{m=-\infty}^{\infty} \sigma_m\, e^{-j2\pi mx/p}\, e^{-j\kappa x}, \\ E_x(x) &= \sum_{m=-\infty}^{\infty} E_m\, e^{-j2\pi mx/p}\, e^{-j\kappa x}. \end{aligned} \tag{E.27}$$

Here the total field $E_x(x)$ includes a component $E_i(x)$ corresponding to the potential $\phi_i(x)$ of equation (E.25), so that

$$E_i(x) = j\kappa\phi_{i0} \exp(-j\kappa x). \tag{E.28}$$

The remaining part of the field $E_x(x)$ is related to the charge density by the effective permittivity of the material, which in this case is the constant $\varepsilon_0 + \varepsilon_p$, since the material is non-piezoelectric. Thus in this case we have

$$E_m/\sigma_m = jS_m/(\varepsilon_0 + \varepsilon_p), \quad \text{for } m \neq 0 \tag{E.30}$$

and

$$(E_0 - j\kappa\phi_{i0})/\sigma_0 = j/(\varepsilon_0 + \varepsilon_p), \tag{E.31}$$

where S_m is defined in equation (D.6). With these equations, the field and charge density may be found using the method given in Appendix D. The coefficients σ_m and E_m are expressed in terms of Legendre polynomials using coefficients α_{-1}, α_0 and α_1, as in equations (D.11)–(D.13). Here, equation (E.30) is satisfied if $\alpha_{-1} = 0$, so only the α_0 and α_1 terms are required. Using equation (E.31) gives α_1, which is found to be

$$\alpha_1 = -j\kappa\phi_{i0}/2. \tag{E.32}$$

The value of α_0 depends on the electrical terminations. As in Appendix D, the electrode voltages and currents are $V_n = V_0 \exp(-j\kappa np)$ and $I_n = I_0 \exp(-j\kappa np)$, and V_0 and I_0 are given respectively by equations (D.21) and (D.23) with $\alpha_{-1} = 0$. Here we assume that the electrodes are either shorted ($V_0 = 0$) or open-circuited ($I_0 = 0$), and it follows that α_0 is given by

$$\alpha_0 = \pm \tfrac{1}{2}j\kappa\phi_{i0}P_s(\pm\cos\Delta)/P_{-s}(\pm\cos\Delta), \tag{E.33}$$

taking the upper signs for open-circuited electrodes and the lower signs for shorted electrodes. Here $s = \kappa p/(2\pi)$ and $\Delta = \pi a/p$.

The charge density $\sigma_1(x)$ is given by equation (D.12), with $\alpha_{-1} = 0$. For subsequent analysis we need the Fourier transform of the charge density on electrode n, evaluated at $\beta = \kappa$, and this is given by

$$\int_{np-a/2}^{np+a/2} \sigma_1(x)\, e^{-j\kappa x}\, dx = -jp(\varepsilon_0 + \varepsilon_p)\, e^{-2jn\kappa p}[\alpha_0 P_{-2s}(\cos\Delta) + \alpha_1 P_{2s}(\cos\Delta)]. \tag{E.34}$$

This is readily obtained from equation (D.12) with the aid of equation (C.16) of Appendix C.

(b) Second-order Green's Function Analysis. In Chapter 4 the Green's function method was used for transducer analysis, and the quasi-static approximation was used. Here a more accurate analysis is needed. For clarity, the quasi-static equations are summarised first.

For a finite array of electrodes with arbitrary voltages, the total surface potential $\phi(x)$ and the charge density $\sigma(x)$ are related by

$$\phi(x) - \phi_i(x) = [G_e(x) + G_s(x, \omega)] * \sigma(x). \tag{E.35}$$

This is the same as equation (4.18) of Chapter 4, except that a potential $\phi_i(x)$ due to

an incident surface wave has been included. $G_e(x)$ and $G_s(x, \omega)$ are respectively the electrostatic and surface-wave Green's functions. For the quasi-static approximation we take $\sigma(x) \approx \sigma_e(x) + \sigma_a(x)$ and neglect a small term $G_s(x, \omega) * \sigma_a(x)$, so that

$$\phi(x) - \phi_i(x) = [G_e(x) + G_s(x, \omega)] * \sigma_e(x) + G_e(x) * \sigma_a(x). \quad \text{(E.36)}$$

The electrostatic term $\sigma_e(x)$ is defined such that $G_e(x) * \sigma_e(x) = \phi(x)$ on the electrodes, which implies that $\sigma_e(x)$ vanishes if the electrode voltages are all the same. Defining the acoustic potential

$$\phi_a(x) = G_s(x, \omega) * \sigma_e(x) \quad \text{(E.37)}$$

as in Chapter 4, equation (E.36) requires $G_e(x) * \sigma_a(x)$ to be equal to $-\phi_i(x) - \phi_a(x)$ on the electrodes. It follows that the acoustic contribution to the charge density is

$$\sigma_a(x_i) = -\sum_j B_{ij}[\phi_i(x_j) + \phi_a(x_j)], \quad \text{(E.38)}$$

where B_{ij} is the electrostatic matrix defined in equation (4.29) and the points x_j exist only on the electrodes, where their spacing is Δx.

The *second-order* solution is obtained by writing

$$\sigma(x) \approx \sigma_e(x) + \sigma_a(x) + \sigma'_a(x), \quad \text{(E.39)}$$

where $\sigma_e(x)$ and $\sigma_a(x)$ are the same functions as before. Substituting into equation (E.35), we exclude a small term $G_s(x, \omega) * \sigma'_a(x)$, but include the term $G_s(x, \omega) * \sigma_a(x)$ which was previously omitted. Thus

$$\phi(x) - \phi_i(x) = [G_e(x) + G_s(x, \omega)] * [\sigma_e(x) + \sigma_a(x)] + G_e(x) * \sigma'_a(x). \quad \text{(E.40)}$$

We define

$$\phi'_a(x) = G_s(x, \omega) * \sigma_a(x). \quad \text{(E.41)}$$

Now, since the potentials on the left of equations (E.36) and (E.40) must be the same on the electrodes, $G_e(x) * \sigma'_a(x)$ must be equal to $-\phi'_a(x)$ on the electrodes, and hence

$$\sigma'_a(x_i) = -\sum_j B_{ij}\phi'_a(x_j). \quad \text{(E.42)}$$

This gives the charge density in the second-order approximation. It is convenient to define a potential

$$\phi_s(x) = \phi_i(x) + \phi_a(x) + \phi'_a(x). \quad \text{(E.43)}$$

In the unmetallised regions this function includes all the terms proportional to $\exp(\pm jk_0x)$, and may therefore be interpreted as the surface wave potentials in these regions.

The current entering electrode n is $I_n = I_{en} + I_{an}$, where I_{en} is the electrostatic term due to $\sigma_e(x)$, and can be found by methods given in Chapter 4. The acoustic term I_{an}, due to $\sigma_a(x)$ and $\sigma'_a(x)$, can be written

$$I_{an} = j\omega W \sum_j \hat{p}_n(x_j)[\sigma_a(x_j) + \sigma'_a(x_j)]\,\Delta x, \quad \text{(E.44)}$$

where $\hat{p}_n(x)$ is unity on electrode n and zero elsewhere. Using equations (E.38) and (E.42) and taking the limit $\Delta x \to 0$, this gives

$$I_{an} = -j\omega W \int_{-\infty}^{\infty} \varrho_{en}(x)\phi_s(x)\,dx, \tag{E.45}$$

where $\phi_s(x)$ is defined by equation (E.43) and $\varrho_{en}(x)$, given by equation (4.32), is the electrostatic charge density on the array when unit voltage is applied to electrode n with the other electrodes grounded. This is very similar to the quasi-static result, equation (4.43).

(c) Reflection Coefficient for Shorted Electrodes. We now consider the reflection coefficient for one electrode in an array of regular electrodes, with pitch p and width a. From equations (E.43), (E.37) and (E.41), the surface-wave potential $\phi_s(x)$ can be written

$$\phi_s(x) = \phi_i(x) + G_s(x, \omega) * [\sigma_e(x) + \sigma_a(x)]. \tag{E.46}$$

The function $\phi_i(x)$ represents a surface-wave potential which would exist in the absence of the electrodes, and therefore has the form

$$\phi_i(x) = \phi_{i0} \exp(-jk_0x), \tag{E.47}$$

where k_0 is the free-square wavenumber. The surface-wave Green's function $G_s(x, \omega)$ is equal to $j\Gamma_s \exp(-jk_0|x|)$. At any x, the convolution in equation (E.46) gives terms proportional to $\exp(-jk_0x)$ and $\exp(jk_0x)$, representing waves propagating in the $+x$ and $-x$ directions respectively. We consider the waves propagating in the $-x$ direction and evaluate these on either side of electrode n. Using the notation of Section E.1, we define b_n as the surface-wave potential at $x = np + p/2$ and b_{n-1} as the potential at $x = np - p/2$. Using equation (E.46), these are related by

$$b_{n-1}\,e^{jk_0p} - b_n = j\Gamma_s\,e^{jk_0(np+p/2)} \int_n [\sigma_e(x') + \sigma_a(x')]\,e^{-jk_0x'}\,dx', \tag{E.48}$$

where the integral is taken over electrode n, so that the limits are $np \pm a/2$. A similar relation can be obtained for waves propagating in the $+x$ direction.

An approximate value for the reflection coefficient is obtained by assuming that, in the vicinity of electrode n, the acoustic potentials $\phi_a(x)$ and $\phi_a'(x)$ in equation (E.43) are much smaller than the incident wave potential $\phi_i(x)$. Thus the wave incident on electrode n from the left, evaluated at $x = np - p/2$, is $\phi_i(np - p/2)$. The electrode reflection coefficient, r, gives the reflected wave amplitude when there is no wave incident from the right, that is, when $b_n = 0$. Referring r to the centre of the electrode, as in Section E.1, we thus have

$$b_{n-1} = r\phi_i(np - p/2)\,e^{-jk_0p} = r\phi_{i0}\,e^{-jk_0(np+p/2)}, \tag{E.49}$$

when $b_n = 0$. The reflection coefficient r may therefore be found from the charge density using equation (E.48). In the present case $\sigma_e(x) = 0$ because the electrodes are taken to be shorted. Furthermore, from equation (E.36) the term $\sigma_a(x)$ is the charge density such that the incident potential $\phi_i(x)$ is cancelled at the electrode locations, calculated using the electrostatic Green's function $G_e(x)$. Thus $\sigma_a(x)$ can be identified as the function $\sigma_1(x)$ of Section E.2(a) above, taking $\kappa = k_0$ in order to comply with equation (E.47). It is also necessary to replace ε_p by $\varepsilon_p^{t'}$ since the material is now piezoelectric. The integral required in equation (E.48) is given by Equation (E.34),

where α_0 and α_1 are respectively given by Equations (E.32) and (E.33); the lower signs are used in equation (E.33) since the electrodes are shorted. The reflection coefficient is thus found to be

$$r \approx -\tfrac{1}{2}j\frac{\Delta v}{v}k_0 p\left[P_{2s}(\cos\Delta) + \frac{P_s(-\cos\Delta)}{P_{-s}(-\cos\Delta)}P_{-2s}(\cos\Delta)\right], \qquad \text{(E.50)}$$

where the relation $(\varepsilon_0 + \varepsilon_p^T)\Gamma_s = \Delta v/v$ has been used, and $s = k_0 p/(2\pi)$. In view of equation (E.26) this is valid only for $0 \leqslant k_0 \leqslant 2\pi/p$, that is, for $\omega \leqslant 2\pi v_0/p$. The solution for higher frequencies is given by Datta and Hunsinger [479]. Strictly, equation (E.50) applies only if the array is infinite, since this was assumed in the derivation of $\sigma_1(x)$. However, for a finite array the same formula may be used if end effects are neglected.

For an infinite array of electrodes the first stop band occurs for frequencies close to the value where $k_0 p = \pi$, that is, where $s = \frac{1}{2}$. At this frequency we find

$$r = -\tfrac{1}{2}j\pi\frac{\Delta v}{v}F_-(\Delta), \quad \text{for } s = \tfrac{1}{2} \qquad \text{(E.51)}$$

where $F_-(\Delta)$ is defined in Appendix D, equation (D.37). Figure D.3 shows $F_-(\Delta)$ as a function of the metallisation ratio. It is seen that $F_-(\Delta)$, and hence the magnitude of r, has a maximum at $a/p = 0.25$. According to the analysis of Appendix D the width of the stop band is $\omega_1 - \omega_{sc}$, given by equation (D.41), and it follows that $\omega_1 - \omega_{sc} = 2v_0|r|/p$. This agrees with the result obtained from the reflective array model, equation (E.16). The reflection coefficient of equation (E.50) is shown as a function of frequency in Figure E.4, for $a/p = \frac{1}{2}$.

(d) Reflection Coefficient for Open-Circuited Electrodes. This can be deduced in a manner very similar to the above analysis for shorted electrodes. The scattering due to electrode n is described by equation (E.48), but here the electrostatic charge density $\sigma_e(x)$ is non-zero because the electrode voltages are finite. It can be assumed that $\sigma_a(x)$ is negligible in comparison with $\sigma_e(x)$, and that $\sigma_e(x)$ is approximately equal to $\sigma_1(x)$ of Section E.2(a). Equation (E.33) is used for α_0, taking the upper signs. Using the same methods as before, the reflection coefficient is found to be

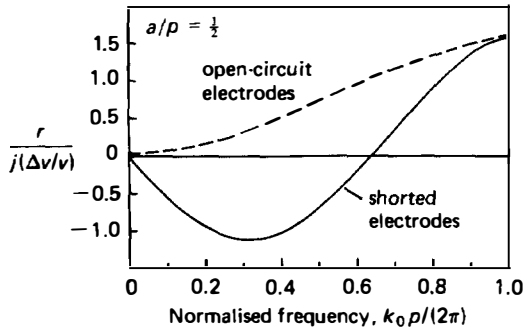

FIGURE E.4. Reflection coefficient for one electrode in a regular array.

$$r \approx -\tfrac{1}{2}j\frac{\Delta v}{v}k_0 p\left[P_{2s}(\cos\Delta) - \frac{P_s(\cos\Delta)}{P_{-s}(\cos\Delta)}P_{-2s}(\cos\Delta)\right]. \qquad \text{(E.52)}$$

For $s = \frac{1}{2}$ we have $r = \frac{1}{2}j\pi(\Delta v/v)F_+(\Delta)$, where $F_+(\Delta)$ is defined in equation (D.37) and shown in Figure D.3. The width of the stop band, given by equation (D.44), is again related to the electrode reflection coefficient by equation (E.16). Figure E.4 shows r as a function of frequency.

A finite array of the open-circuited electrodes has the same structure as the basic multi-strip coupler described in Chapter 5, where the reflection of incident waves by the coupler was ignored. However, for a uniform incident wave the reflection coefficient can be obtained from the reflective array model, equation (E.24), using equation (E.52) for r.

E.3. Electrical Loading in Transducers

In this section we consider interactions in an interdigital transducer with regular electrodes. The transducer is taken to be shorted, and to have a surface wave incident on it. The wave amplitudes throughout the transducer can in principle be obtained using the Green's function method of Section E.2. However, owing to the approximations used the resulting expressions do not conserve the power. It is therefore more appropriate to use the reflective array model of Section E.1, taking the electrode reflection coefficient r to be given by the approximate result of equation (E.50). For consistency, the electrode transmission coefficient, t, must be related to r by equations (E.4) and (E.7), where the ambiguity of sign is resolved by noting that t must be close to unity. Since r is imaginary, this implies that t must be real. Consequently, at frequencies where interaction effects are not significant the analysis will predict that the surface-wave velocity within the structure will be the free-surface velocity v_0. This is in fact erroneous, since the velocity will have a value between v_0 and v_m, dependent on the metallisation ratio, as shown in Section D.2. However, the analysis here is readily corrected for the velocity error by adjusting the value of k_0.

(a) Reflection Coefficient. When the transducer is shorted, the polarities of the electrodes have no effect on the reflection coefficient, so the latter is the same as for a simple array of shorted regular electrodes. The reflection coefficient is therefore given by equation (E.24), using equation (E.50) for the electrode reflection coefficient r. Measurements on an array of electrodes can therefore be used to confirm the theoretical expression for r, though care is needed if a large number of electrodes is used since this can give significant propagation losses not allowed for in the reflective array model of Section E.1. For a regular array, significant reflections occur for $s = \frac{1}{2}$, that is, when the pitch equals half the wavelength, and for $s = \frac{1}{2}$ and $a/p = \frac{1}{2}$ equation (E.50) gives $r = -0.718j\Delta v/v$. For Y, Z lithium niobate, with $\Delta v/v = 2.15\%$, we thus have $|r| = 0.0154$. This is confirmed by measurements on arrays of aluminium electrodes [494, 495]. The variation of r with a/p, shown by

equation (E.51) and Figure D.3, is also confirmed experimentally [494]. In addition, it is found that the value of r is independent of the film thickness [495], confirming the assumption that the reflection is predominantly due to electrical, rather than mechanical, loading. The theoretical reflection coefficient for $N = 40$ electrodes with $a/p = \frac{1}{2}$ is shown as a function of frequency in Figure E.3. This is similar to De Vries' measurement [496, p. 276] on a shorted transducer, though the maximum value of 0.55 is somewhat larger than the experimental maximum of 0.44.

(b) Frequency Response. The transducer response is found by a method similar to that described by Skeie and Engan [485]. The analysis here is valid for an apodised transducer, but for convenience we assume initially that the transducer is unapodised. We consider the output current I_{sc} produced when the transducer is shorted and a surface wave is incident. Since the electrodes are shorted the electrostatic charge density $\sigma_e(x)$ is zero, and consequently the current I_n flowing into electrode n consists only of the acoustic term I_{an}, which is given by Equation (E.45). In the present case the electrodes are regular and electrode n is centred at $x = np$, so that $\varrho_{en}(x)$ can be replaced by $\varrho_f(x - np)$, giving

$$I_n = -j\omega W \int_{-\infty}^{\infty} \varrho_f(x - np)\, \phi_s(x)\, \mathrm{d}x, \tag{E.53}$$

where $\phi_s(x)$ is the surface-wave potential, defined by equation (E.43). The elemental charge density $\varrho_f(x - np)$ is small except in the vicinity of electrode n. Now, if the interactions are not too strong the surface-wave amplitude will not vary rapidly with distance, so the waves in the vicinity of electrode n are approximately proportional to exp $(\pm jk_0x)$. In the analysis of Section E.1 the waves incident on electrode n are given by c_{n-1}, measured at $x = np - p/2$, and b_n, measured at $x = np + p/2$. Taking these as surface-wave potentials, the total surface-wave potential in the vicinity of electrode n is approximately given by

$$\phi_s(x) \approx c_{n-1}\, \mathrm{e}^{-jk_0(x - np + p/2)} + b_n\, \mathrm{e}^{jk_0(x - np - p/2)}.$$

Substituting into equation (E.53), the integral can be expressed in terms of the Fourier transform of $\varrho_f(x)$, denoted by $\bar{\varrho}_f(\beta)$. Noting that $\bar{\varrho}_f(-\beta) = \bar{\varrho}_f(\beta)$, this gives

$$I_n = -j\omega W \bar{\varrho}_f(k_0)[c_{n-1} + b_n] \exp(-jk_0p/2), \tag{E.54}$$

The above equation gives the current entering electrode n, for an unapodised shorted transducer of aperture W. We now generalise to an *apodised* transducer, assuming that dummy electrodes are included as in, for example, Figure 8.1. The electrode breaks are taken to be much smaller than W. Since the transducer is shorted, the surface wave amplitudes within it will not be affected by the apodisation, and

hence equation (E.54) gives the total current entering the electrodes centred at $x = np$. The current entering from the upper bus-bar, denoted I_n', is proportional to the length u_n of the electrode connected to this bus-bar, so that

$$I_n' = -j\omega u_n \bar{\varrho}_f(k_0)[c_{n-1} + b_n] \exp(-jk_0 p/2) \tag{E.55}$$

and the total current flowing in the short-circuit connected to the transducer is

$$I_{sc} = \sum_{n=1}^{N} I_n', \tag{E.56}$$

where N is the number of electrodes.

For simplicity it is assumed here that the transducer geometry is symmetrical, and that N is odd. The method given below is readily adapted for the case of an anti-symmetrical geometry, and the two cases can be combined to analyse a more general geometry [485]. The total current is written as

$$I_{sc} = \sum_{n=1}^{(N-1)/2} (I_n' + I_{N-n+1}'),$$

where, for simplicity, the current in the central electrode, with $n = (N + 1)/2$, has been omitted. For a symmetrical transducer $u_{N-n+1} = u_n$, and using equation (E.55) we have

$$I_{sc} = -j\omega\bar{\varrho}_f(k_0)\, \mathrm{e}^{-jk_0 p/2} \sum_{n=1}^{(N-1)/2} u_n(c_{n-1} + b_n + c_{N-n} + b_{N-n+1}). \tag{E.57}$$

Using equation (E.22) for c_n and equation (E.23) for b_n, it is found that this can be written in the form

$$I_{sc}/c_0 = H_0(\gamma)A(\gamma). \tag{E.58}$$

Here c_0 is the potential of the incident surface wave at $x = p/2$, which can be taken as the location of the acoustic port (the first electrode is centred at $x = p$). The functions on the right are

$$H_0(\gamma) = -2j\omega\bar{\varrho}_f(k_0)\, \mathrm{e}^{-jN\gamma p/2} \sum_{n=1}^{(N-1)/2} u_n \cos(N - 2n + 1)\gamma p/2 \tag{E.59}$$

and

$$A(\gamma) = \frac{\sin(N + 1)\gamma p/2 - \tau(1 - r/t)\sin(N - 1)\gamma p/2}{\sin N\gamma p - \tau \sin(N - 1)\gamma p}\, \mathrm{e}^{j(N-1)\gamma p/2}. \tag{E.60}$$

The ratio I_{sc}/c_0 is essentially the transducer frequency response, as can be seen by comparison with equation (4.122). The interaction effects disappear if we put $r = 0$

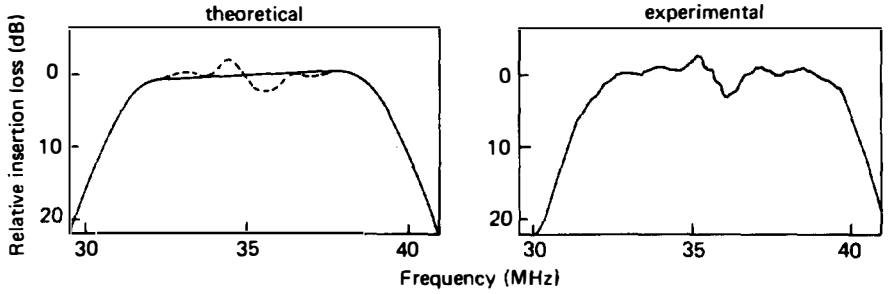

FIGURE E.5. Insertion loss of an interdigital device, showing ripple due to electrode interactions (Courtesy, Plessey Research).

and $\gamma = k_0$. With these values equation (E.60) gives $A(k_0) = 1$, so that $I_{sc}/c_0 = H_0(k_0)$; this is found to be consistent with the quasi-static analysis in Chapter 4, equtions (4.129) and (4.122). When interactions are significant, the function $H_0(\gamma)$ is similar to the first-order response $H_0(k_0)$; the distortion arises mainly from the function $A(\gamma)$. The amplitude distortion is given by $|A(\gamma)|$, and for $\gamma p < 2\pi$ this is close to unity except when γp is close to π.

Figure E.5 shows, on the right, the experimental insertion loss of a device using aluminium electrodes on a Y, Z lithium niobate substrate. The ripple is due to electrode interactions. The device consisted of an apodised single-electrode transducer with $N = 51$ electrodes, and an unapodised double-electrode transducer, the latter giving negligible electrode interactions. The metallisation ratio was 0.5. The continuous theoretical curve shows the response calculated by the quasi-static method of Chapter 4, that is, ignoring electrode interactions. The experimental device was connected directly to the electrical source and load without intervening matching components, and consequently circuit effects are small. The distortion due to interactions can therefore be obtained directly from equation (E.60), using

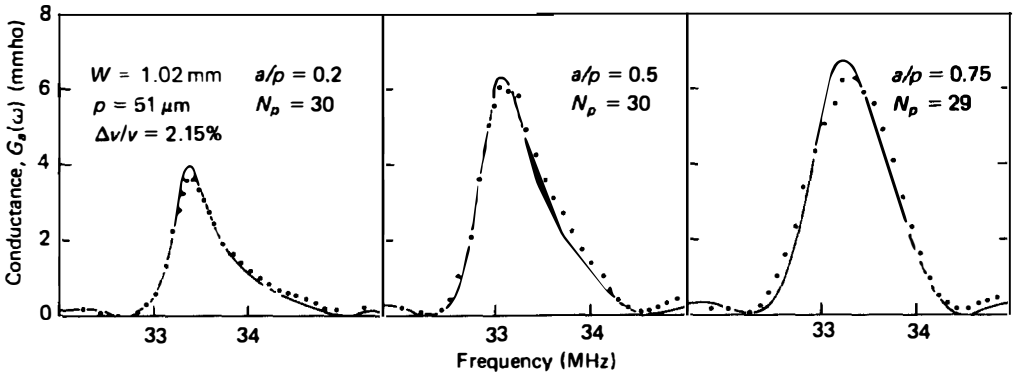

FIGURE E.6. Parallel conductance of single-electrode transducers. Experimental points from Daniel and Emtage [497], with permission.

equation (E.50) for r and taking $\Delta v/v = 2.15\%$. This gives the broken theoretical curve in Figure E.6, agreeing well with the experimental result. Similar experimental and theoretical results were obtained by Skeie and Engan [485].

(c) Conductance of an Unapodised Transducer. Electrode interactions also distort the parallel conductance $G_a(\omega)$ of a transducer. Here we consider only an unapodised transducer, though the method may be extended to the case of an apodised transducer by using parallel channels (Section 4.7.2). For an unapodised transducer, the potential ϕ_{s1} of the wave launched at the acoustic port when a voltage V_t is applied can be obtained by reciprocity, equation (B.24), giving

$$\phi_{s1} = -V_t \frac{\Gamma_s}{\omega W} \frac{I_{sc}}{c_0},$$

where I_{sc}/c_0 is given by equation (E.58). The power carried by this wave is given by equation (3.34) of Chapter 3, and since the transducer is here taken to have a symmetrical geometry an equal power is carried by the wave launched at port 2. The total surface wave power is accounted for by the conductance $G_a(\omega)$, and we thus find

$$G_a(\omega) = \Gamma_s |H_0(\gamma) A(\gamma)|^2/(\omega W). \tag{E.61}$$

This function is shown, for uniform single-electrode transducers, in Figure E.6. The experimental points were obtained by Daniel and Emtage [497], using aluminium transducers on a Y, Z lithium niobate substrate, with metallisation ratios $a/p = 0.2$, 0.5 and 0.75. The number of periods, N_p, was 29 for $a/p = 0.75$ and 30 for the other cases. The aperture W and pitch p were the same for all three transducers. The theoretical curves use equations (E.59) and (E.60) and, because of a small uncertainty in the transducer period, have been displaced along the frequency axis to fit the experimental data. Daniel and Emtage [497] obtained similar theoretical curves. If electrode interactions were negligible the conductance would be an approximately symmetrical function, as shown for example by Figure 4.14. The interactions cause considerable distortion, and the distortion is greatest for $a/p = 0.2$, becoming progressively weaker for $a/p = 0.5$ and 0.75. This is due to the variation of the electrode reflection coefficient r. For $s = \frac{1}{2}$, that is, at the transducer centre frequency, r is proportional to the function $F_-(\Delta)$ shown in equation (E.51) and Figure D.3, and its magnitude is maximised at $a/p = 0.25$. The experimental results therefore confirm the theoretical variation of r with a/p, as well as confirming the analysis for electrode interactions.

E.4. Mechanical Loading

Up to this point we have only considered interactions due to electrical loading. However there are in addition perturbations of a mechanical nature, present even if the substrate is not piezoelectric. There are two types of mechanical perturbation. Firstly, the presence of electrodes on the surface alters the surface geometry, giving

a perturbation sometimes called the "topographic effect". This occurs if a set of grooves is etched into the surface. Secondly, an additional perturbation occurs in the case of deposited strips of metal or dielectric material, because the elastic properties differ from those of the substrate; this is often called "mass loading". In practical devices the metal film used for transducers is chosen to have elastic properties similar to the substrate in order to minimise mass loading effects, and usually this implies the choice of an aluminium film. The term "mechanical loading" is used here to include both topographic effects and mass loading.

For metal electrodes on a piezoelectric substrate, both electrical loading and mechanical loading are present. However, for strongly piezoelectric substrates such as lithium niobate, mechanical loading is usually negligible in comparison with electrical loading, and may therefore be ignored as in the analysis above. For weakly piezoelectric substrates, such as quartz, mechanical loading usually dominates. Intermediate cases, where both types of loading are relevant, do not often occur in practice, so here only mechanical loading is considered.

As in the case of electrical loading, the scattering properties of an array of regular electrodes are related to the scattering due to one electrode by the reflective array model of Section E.1, and the relevant transducer properties are given by the analysis in Section E.3. Thus, here it is only necessary to consider the electrode reflection coefficient r and the effective velocity for surface waves in the structure.

The analysis for mechanical loading has been considered by several authors [483, 486, 498–501]. Neglecting piezoelectricity, it is found that to first order the reflection coefficient for one electrode is approximately given by [486, 499, 500]

$$r \approx 2j\alpha_r(h/\lambda) \sin(ak), \tag{E.62}$$

where α_r is a real constant, $k \approx k_0$ is the surface-wave wavenumber, $\lambda = 2\pi/k$ is the wavelength, and a and h are respectively the width and thickness of the electrode. It is assumed that $h \ll \lambda$. The formula applies irrespective of the proximity of any adjacent electrodes. It can be interpreted in terms of a reflection coefficient $\alpha_r h/\lambda$ for the leading edge of the electrode, and an equal and opposite reflection coefficient for the trailing edge. As a function of the width a, the reflection coefficient has a maximum value of $2j\alpha_r h/\lambda$ when $a = \lambda/4$.

For the common experimental case of aluminium electrodes on a ST, X quartz substrate, analysis [486, 500] gives 0.28 or 0.25 for the value of α_r. Experimental measurements [502, 503], using arrays of electrodes with $a \approx \lambda/4$, gave values of 0.25 and 0.33, in reasonable agreement. Further, Marshall [502] showed experimentally that the reflection coefficient is proportional to h, in agreement with equation (E.62), thus confirming that mechanical loading is the main cause of the perturbation. For transducers operating at 100 MHz, say, a typical value of h/λ is 0.01, giving $|r| \approx 0.006$. This is considerably less than the reflection coefficient for aluminium electrodes on lithium niobate, and hence electrode interactions are generally weaker when quartz substrates are used.

Skeie [483] has investigated transducers on Y, Z lithium niobate using gold metallisation. This case was found to give substantial mechanical loading, so that the electrode interactions were considerably stronger than for electrical loading alone.

Thus aluminium is generally preferable to gold.

In addition to reflections, mass loading also causes a phase change of a surface wave transmitted through an electrode. For an array of regular electrodes, and for frequencies outside the stop bands, this is equivalent to a change of surface-wave velocity. According to first-order analysis [501] the velocity varies linearly with the metallisation ratio a/p, and can therefore be calculated straightforwardly from the velocity perturbation due to a continuous film. This gives a velocity perturbation proportional to h/λ. However, Datta and Hunsinger [501] have shown that there is in addition a second-order, or "stored energy", term proportional to $(h/\lambda)^2$. For aluminium electrodes on *ST*, *X* quartz this will usually be larger than the first-order term. A 337 MHz double-electrode transducer with 900 Å metallisation gave an experimental velocity perturbation of 0.24%, and the analysis gave good agreement.